Chemical Science

ROYAL SOCIETY OF CHEMISTRY

EDGE ARTICLE

View Article Online
View Journal | View Issue

Cite this: *Chem. Sci.*, 2025, **16**, 3307

All publication charges for this article have been paid for by the Royal Society of Chemistry

Introducing halogen-bonded gates into zeolitic frameworks for efficient benzene/cyclohexene/cyclohexane separation†

Zi-Jun Liang,‡ Fang-Di Dong,‡ Le Ye, Kai Zheng, Ding-Yi Hu, Xi Feng, Wen-Yu Su, Zhi-Shuo Wang, Mu-Yang Zhou, Zi-Luo Fang, Dong-Dong Zhou, * Jie-Peng Zhang * and Xiao-Ming Chen

Received 30th September 2024
Accepted 14th January 2025

DOI: 10.1039/d4sc06624c

rsc.li/chemical-science

The separation of C_6 cyclic hydrocarbons (benzene, cyclohexene, and cyclohexane) is one of the most challenging chemical processes in the petrochemical industry. Herein, we design and synthesize a new SOD-topology metal azolate framework (MAF) with aperture gating behaviour controlled by C–Br···N halogen bonds, which exhibits distinct temperature- and guest-dependent adsorption behaviours for benzene/cyclohexene/cyclohexane. More importantly, the MAF enables the efficient purification of benzene from its binary and ternary mixtures (selectivity up to 113 ± 2; purity up to 98% +), which is the highest record for benzene/cyclohexane/cyclohexene separation to date. Single-crystal diffraction analyses and computational simulations revealed that halogen bonds play a critical role in the gating and diffusion process, which is the first example of halogen-bonding controlled gating for highly effective adsorptive separation.

Introduction

Hydrogenation products of benzene (Bz), *i.e.*, cyclohexene (Cye) and cyclohexane (Cya), are the raw materials for producing nylon-6 and nylon-66, which play an important role in the textile and plastics industries.[1–4] To avoid complete hydrogenation, the process generally yields a Bz/Cye/Cya mixture, particularly during the industrial preparation of Cye, where the yield is only ~60% with Cya as the byproduct,[5] necessitating their subsequent separation. However, their close boiling points (Bz: 353.3 K, Cya: 353.9 K, and Cye: 356.0 K) and their tendency to form azeotropes make conventional methods that employ extractive distillation energy-intensive and complex.[6,7] Alternatively, adsorptive separation based on porous materials is a promising way to realize lower energy consumption and higher efficiency.[8–14]

Porous coordination polymers (PCPs) or metal–organic frameworks (MOFs) exhibit potential applications in adsorptive separation due to their high specific surface areas and highly designable/modifiable structures.[15–24] In addition, compared to conventional porous materials, MOFs possess unique flexibility, offering new possibilities for efficient separation.[25–31] As one of the most studied materials, SOD-[Zn(mim)$_2$] (MAF-4, also known as ZIF-8, Hmim = 2-methylimidazole) is a three-dimensional (3D) framework with zeolite SOD topology.[32] Although the crystallographic diameter of pore apertures, *i.e.*, the six-membered rings (6 MR) of $Zn_6(mim)_6$, is only 3.4 Å, it can open transiently *via* ligand rotation/swing (*i.e.*, aperture gating flexibility)[33–38] to allow the diffusion and adsorption of molecules as large as xylene and can achieve a selectivity of *ca.* 2–10.[39] By applying an external electric field or introducing bulkier 2-position substituent groups,[40] the ligand rotation/swing could be restricted to enhance C_3H_6/C_3H_8 selectivity by ~30%.[35,41–44] In principle, introducing a substituent group onto the 4-/5-position of imidazolate can directly reduce the size of the 6 MR aperture and increase the gating energy barrier. However, since the 6 MR aperture is already quite small, introducing a substituent group onto the 4-/5-position of imidazolate generally changes the network topology.[45] The only exception is [Zn(bim)$_2$] (MAF-3, also known as ZIF-7, Hbim = benzimidazole) with a fused phenyl group,[46] which still possesses the SOD topology, but the coordination framework is highly distorted, leading to very small porosity. Moreover, introducing additional intra-framework interactions (*e.g.*, hydrogen bonds) can also regulate the energy barrier of aperture gating.[47] For example, halogen bonds, similar to hydrogen bonds, theoretically can also modulate the aperture gating process, but no reports have been published thus far.

MOE Key Laboratory of Bioinorganic and Synthetic Chemistry, School of Chemistry, GBRCE for Functional Molecular Engineering, IGCME, Sun Yat-Sen University, Guangzhou 510275, China. E-mail: zhoudd3@mail.sysu.edu.cn; zhangjp7@mail.sysu.edu.cn

† Electronic supplementary information (ESI) available. CCDC 2386982 and 2386983. For ESI and crystallographic data in CIF or other electronic format see DOI: https://doi.org/10.1039/d4sc06624c

‡ These authors contributed equally to this work.

Here, we report a new SOD MOF or MAF-4 analogue, *i.e.*, $[Zn(btz)_2]$ (MAF-7Br, Hbtz = 3-bromo-1,2,4-triazole). After introducing the large Br atoms and Br···N bonds in the 6 MR aperture, MAF-7Br showed molecular-sieving-like separation of Bz from Bz/Cye/Cya mixtures, making it the new benchmark Bz-selective material.

Results and discussion

The solvothermal reaction of $Zn(NO_3)_2 \cdot 6H_2O$ and Hbtz in *N*,*N*-dimethylformamide (DMF) at 373 K yielded the colourless rhombic dodecahedral single crystals of MAF-7Br. Similarly, microcrystalline samples of MAF-7Br could be synthesized on the gram scale by stirring at the same temperature with high yield (*ca.* 86%) (Fig. S1†).

Single-crystal X-ray diffraction (SCXRD) revealed that MAF-7Br crystallizes in the cubic space group, the same as that of MAF-4 (Fig. S2, Tables S1†).[32] In MAF-7Br, the btz^- ligands adopt μ-imidazolate coordination mode, leaving one uncoordinated N atom (Fig. 1a, b and S3†), which is the same as that in $[Zn(mtz)_2]$ (MAF-7, Hmtz = 3-methyl-1,2,4-triazole).[48,49] However, in MAF-7Br and MAF-7, the ligands leave the 2- and 1-N atoms uncoordinated, respectively. This results in significant differences in pore apertures (Fig. 1 and S4–S6†). Specifically, the 6 MR aperture in MAF-7Br is defined by three pairs of Br atoms and N atoms showing three typical halogen bonds (Br···N 3.16(2) Å) (Fig. S4a†). Because Br is much larger than H, the aperture size decreases from 3.4 Å in MAF-4 to 0.3 Å in MAF-7Br (Fig. 1c and S6†). In the 6 MR aperture of MAF-7, the H···N distance (4.39 Å) is very long, and the aperture size (3.4 Å) is similar to that of MAF-4 (Fig. 1d and S6†).[32] Although the void ratio and cavity size of MAF-7Br (50.4% and 10.7 Å), MAF-7 (51.7% and 11.2 Å) and MAF-4 (49.8% and 11.4 Å) are similar, the pore systems of MAF-7Br and MAF-7/MAF-4 can be regarded as discrete and 3D, respectively (Fig. 2e, f and S7†).[48]

Powder X-ray diffraction (PXRD) patterns of as-synthesized MAF-7Br and MAF-7 matched well with their simulated ones (Fig. S8†), indicating high purity of the samples. In water, MAF-7 remains stable for only one week, while MAF-7Br remains stable for at least one month (Fig. S9†). This can be attributed to its smaller pore apertures and more hydrophobic –Br groups, which hinder the access of water molecules. Additionally, the PXRD patterns of MAF-7Br remained unchanged after being immersed in HCl (pH = 2) and NaOH (pH = 13) solutions for at least one week (Fig. S9†), further confirming its higher chemical stability. Thermogravimetry (TG) curves showed that the guest of MAF-7 and dichloromethane-exchanged MAF-7Br could be completely removed below 373 K (Fig. S10†). Interestingly, MAF-7Br gradually turned to an amorphous phase (Fig. S8†), but it still maintained its rhombic dodecahedral shape, and its size did not undergo significant changes, becoming only slightly opaque (Fig. S11 and S12†), which suggested that the amorphization should be framework distortion, rather than framework collapse.[50–53] In contrast, MAF-4 and MAF-7 are known to readily adsorb and desorb guests through single-crystal to single-crystal transformations.[33,48]

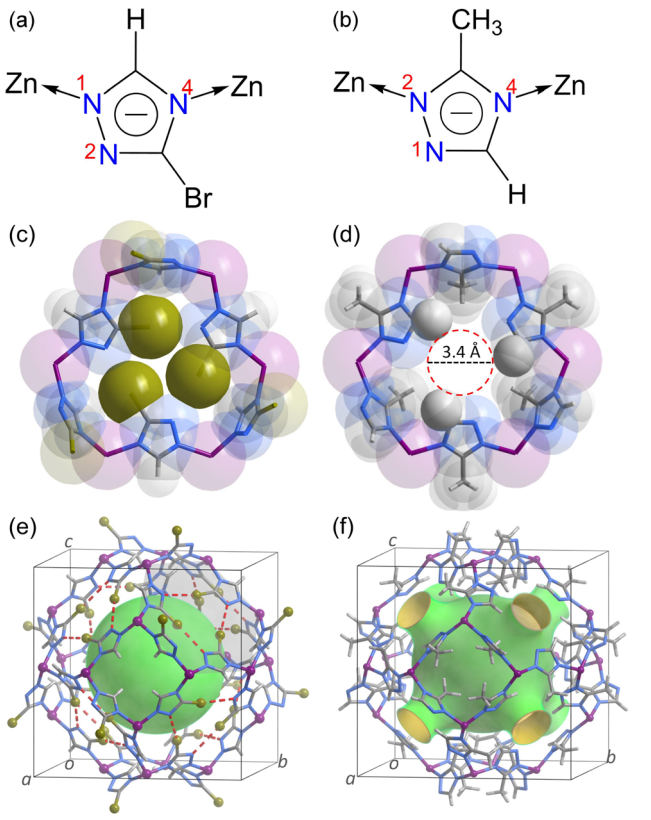

Fig. 1 Single-crystal structures of MAF-7Br and MAF-7. (a and b) The different coordination modes of the triazolate ligands in MAF-7Br (a) and MAF-7 (b). (c and d) The 6 MR apertures in MAF-7Br (c) and MAF-7 (d), with the functional groups (–Br or $-CH_3$ groups) blocking the apertures highlighted in the space-filling mode with less transparency. (e and f) The frameworks and pore structures of MAF-7Br (e) and MAF-7 (f), with the halogen bonds shown as red dashed lines, acting as a gate (light grey colour).

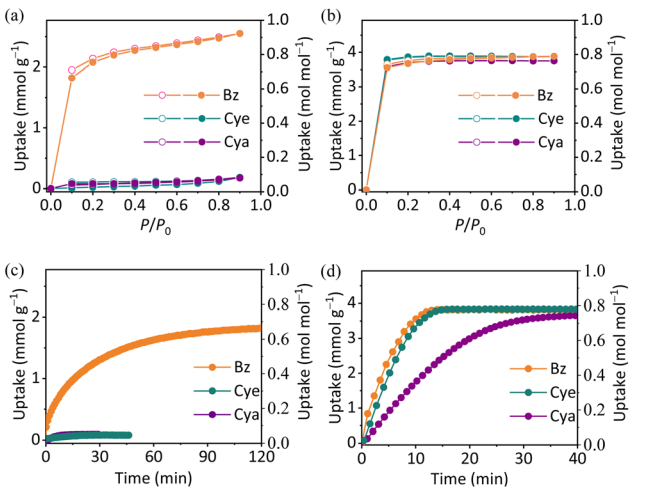

Fig. 2 Bz/Cye/Cya sorption behaviours at 313 K. (a and b) Adsorption and desorption isotherms of MAF-7Br (a) and MAF-7 (b). Solid and open symbols represent adsorption and desorption, respectively. (c and d) Adsorption kinetics of Bz/Cye/Cya for MAF-7Br (c) and MAF-7 (d) at $P/P_0 = 0.1$.

Fortunately, single-crystalline and completely transparent MAF-7Br could be restored by immersing activated MAF-7Br in DMF at room temperature or in Bz at 313 K within 24 h (denoted as Bz@MAF-7Br, Fig. S12†), and the recovery process could be accelerated at higher temperature (Fig. S13 and S14†). In addition, attenuated total reflection Fourier transform infrared (ATR-FTIR) and Raman spectra showed large blue shifts of the peak of ν_{C-Br} in activated MAF-7Br (668 cm^{-1}) and Bz@MAF-7Br (666 cm^{-1}) from that in Hbtz (636 cm^{-1}), indicating the existence of strong halogen bonding (Fig. S15–S17†). Furthermore, except for the additional characteristic peaks of ν_{Bz} and γ_{Bz} in the Bz-loaded sample, the positions of other peaks (including the peaks of ν_{Zn-N}) were almost identical between the activated MAF-7Br and Bz@MAF-7Br, indicating that the structure should not undergo any coordination bond or chemical bond breakage or reconstitution. Solid-state ^{13}C-NMR analysis showed that the activated MAF-7Br exhibited distinct two splitting peaks of C(–Br) compared with that in Bz@MAF-7Br, meaning the presence of more than one type of btz^- after activation (Fig. S18†), which further aligns with the rotational disorder of the btz^- rings. In a word, all spectral results indicated that the amorphization might not break the coordination bond but merely distort the framework. Furthermore, SCXRD analysis indicated that Bz@MAF-7Br and MAF-7Br are isostructural (Fig. S2, S4, S19, and Tables S1†), and each cavity assembles six Bz molecules with an octahedral arrangement (Fig. S20†). In contrast, organic solvents with larger sizes like Cye, Cya, and xylenes could not restore the crystallinity even under boiling conditions (Fig. S21†), implying that MAF-7Br may have potential separation capabilities for Bz/Cye/Cya mixtures.

While MAF-7 showed normal gas adsorption behaviours (similar to MAF-4),[48] MAF-7Br barely adsorbs N_2 or CO_2 (Fig. S22 and S23†). Considering that the morphology and size of the activated MAF-7Br were almost the same as those of the as-synthesized MAF-7Br (Fig. S11†), their internal cavity and void ratio should not differ much and the local structure should be similar. The difficulty in adsorbing gas molecules probably was because the pore aperture of MAF-7Br is too small and the gating barrier is too high. Although gas molecules are small (a small aperture opening is required for diffusion), they interact weakly with the aperture. In contrast, solvent molecules are large (a large aperture opening is required for diffusion). Many examples have shown that strong host–guest interactions are more important for guest diffusion through ultra-small pore apertures (overcoming the gating barrier of the aperture).[47]

Single-component Bz/Cye/Cya sorption isotherms were recorded for MAF-7Br and MAF-7 at 298/313 K. MAF-7 showed a reversible type-I sorption isotherm for Bz/Cye/Cya, with a saturation uptake of *ca.* 4 mmol g^{-1} or 0.88 mol mol^{-1} at 298/313 K (Fig. 2 and S24†).[54] The sorption isotherm of MAF-7Br for Bz also exhibited a similar type-I profile at 313 K, with an uptake of 2.55 mmol g^{-1} or 0.92 mol mol^{-1} at $P/P_0 = 0.90$ (Fig. 2). However, it barely adsorbed Bz at 298 K, with an uptake of 0.32 mmol g^{-1} or 0.18 mol mol^{-1} at 298 K (Fig. S24†). The higher uptake at 313 K indicated that the measured isotherms were not thermodynamic equilibrium data, and the diffusion or adsorption kinetics play a dominant role aligning with the gating flexibility.[47,55–57] In addition, the uptakes of Bz for MAF-7Br were obtained at more temperatures by ^{1}H NMR, and the results showed that the uptake of Bz also increased with temperature below 313 K, but decreased with increasing temperature above 313 K (Fig. S25 and S26†), indicating that it is a typical aperture gating flexibility behaviour.[47,55–57] After multiple adsorption–desorption cycles for Bz, the PXRD patterns, morphology/size, adsorption kinetics and uptake showed no significant change (Fig. S27–S31†).

For Cya/Cye, the uptake of MAF-7Br was 0.32/0.21 and 0.17/0.18 mmol g^{-1} at 298 and 313 K, respectively (Fig. 2 and S24†). Different from Bz, the Cya/Cye uptake did not increase at higher temperature, indicating that the adsorption process was thermodynamically dominated. The energy barrier of diffusion was too high, so Cya/Cye could hardly diffuse at both high and low temperatures, indicating that adsorption occurred on the surface of particles and/or defects rather than in pores, which suggested molecular sieving for Bz/Cya and Bz/Cye mixtures.

Differential scanning calorimetry (DSC) measurements showed that the adsorption enthalpy (ΔH) for Bz/Cye/Cya was −71.7/−68.0/−64.3 kJ mol^{-1} for MAF-7, respectively, and that for Bz was −87.9 kJ mol^{-1} for MAF-7Br (Fig. S32†). In addition, adsorption kinetics measurements showed fast Bz/Cye/Cya adsorption rates in MAF-7 (6.6×10^{-2}/6.5×10^{-2}/2.9×10^{-2} min^{-1}, respectively), in the order of Bz > Cye > Cya. In contrast, the Bz adsorption in MAF-7Br was slow (6.6×10^{-3} min^{-1}), while Cye (7.4×10^{-6} min^{-1}) and Cya (7.2×10^{-6} min^{-1}) hardly adsorbed (Fig. 2 and S33†). PXRD patterns of samples soaked in Bz at different times indicated that the transition from amorphous to crystalline coincided with Bz adsorption (Fig. S14†).

To verify the practical separation performance, MAF-7Br and MAF-7 were immersed in equimolar mixtures of Bz/Cya, Bz/Cye and Bz/Cye/Cya at 313 K. The selectivities were analysed by gas chromatography (GC) measurements of the adsorbate (Fig. 3 and S34–S36†). MAF-7 showed Bz selectivities of 2.2, 1.7, and 1.4 from the Bz/Cya, Bz/Cye and Bz/Cye/Cya mixtures, and Bz purities of only 68.8%, 63.0%, and 41.2% were obtained after one adsorption–desorption process, respectively. MAF-7Br showed Bz selectivities of 43.4 ± 1.6, 65.5 ± 2.8 and 113 ± 2 from the Bz/Cye, Bz/Cya, and Bz/Cye/Cya mixtures, corresponding to Bz purities of 97.6%, 98.5% and 98.2%, respectively. To our knowledge, the Bz/Cye selectivity of MAF-7Br (43.4 ± 1.6) was comparable with that of previously reported benchmark materials, such as BNF-2 (44.5) and Mn-DHBQ (44.8). Furthermore, MAF-7Br is not only one of the few adsorbents capable of separating Bz from its ternary C_6 cyclic hydrocarbon mixture but also exhibits the highest reported Bz selectivity to date (Table S2†).[9,12] In addition, after four consecutive adsorption–desorption cycles of Bz/Cye/Cya mixtures, the morphology/size, uptake/selectivity, and PXRD patterns remained unchanged (Fig. S29, S30 and S37†), indicating that MAF-7Br exhibits high stability and recyclability.

To further elucidate the separation mechanism, various computational simulations were employed. First, grand canonical Monte Carlo (GCMC) simulations showed that each cavity of MAF-7Br/MAF-7 can accommodate six Bz, Cya and Cye

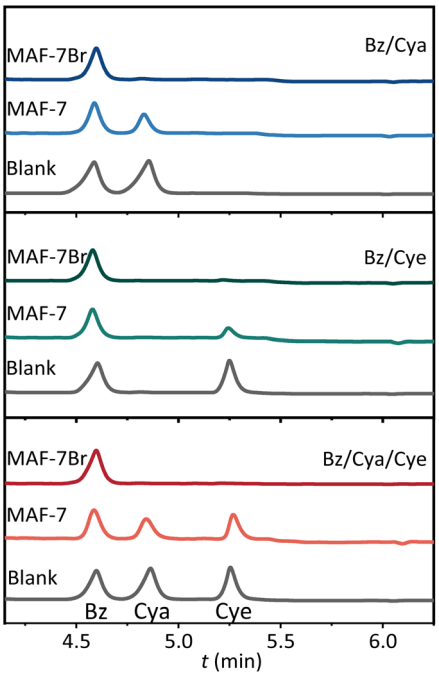

Fig. 3 Typical gas chromatography (GC) traces of the digestion solutions of MAF-7Br and MAF-7 after soaking in equimolar mixtures of Bz/Cya (up), Bz/Cye (middle), and Bz/Cya/Cye (down).

molecules, respectively, corresponding to the same uptake of 1.0 mol mol^{-1}. All preferential adsorption sites were concentrated around the 4 MR (Fig. S38 and Table S3†), which was consistent with the SCXRD result of Bz@MAF-7Br (Fig. S39†). Further, periodic density functional theory (PDFT) calculations estimated the ΔH of Bz, Cye, and Cya for MAF-7Br/MAF-7 to be −90.1/−74.8, −76.0/−73.5 and −73.9/−67.9 kJ mol^{-1}, respectively, consistent with the results of DSC measurements. Obviously, the ultrahigh adsorption selectivity of MAF-7Br should be originated from the kinetics rather than thermodynamics.

According to the sizes of guests and pore apertures, both MAF-7Br and MAF-7 need to instantaneously open the pore aperture (*i.e.*, gating) to allow Bz/Cye/Cya adsorption (Fig. 4), of which the diffusion was revealed by molecular dynamics (MD) simulations. Expectably, if the host was set rigid, the diffusion of Bz/Cye/Cya was forbidden in MAF-7Br and MAF-7 (diffusion rate <2 × 10^{-13} m^2 s^{-1}, Fig. S40 and Table S4†). When the host was set flexible, the diffusion rate for Bz, Cye, and Cya in MAF-7 was 1.4 × 10^{-9}, 1.2 × 10^{-9}, and 0.5 × 10^{-9} m^2 s^{-1}, respectively. Bz could also diffuse in flexible MAF-7Br, but the diffusion rate was only 0.2 × 10^{-9} m^2 s^{-1} (Fig. 4, S41 and Table S4†). However, Cye and Cya still showed negligibly small diffusion rates of 7 × 10^{-13} and 5 × 10^{-13} m^2 s^{-1}, respectively. These simulation results were consistent with the trends of experimental adsorption kinetics, which indicated that the gating barrier of MAF-7Br was much higher than that of MAF-7, and the former was more sensitive to the guest sizes.

Further, the structures and energies of the key stages of the gating process were calculated by PDFT. The results showed that the gating was almost based on the ligand rotation (that is the location of metal ions was almost unchanged, Fig. 4 and S42–S44†). For MAF-7, because the aperture was already relatively large, the gating action needs the ligand rotation of only ~16.9°, ~17.1°, and ~18.0°, giving energy barriers of 50.1, 52.8,

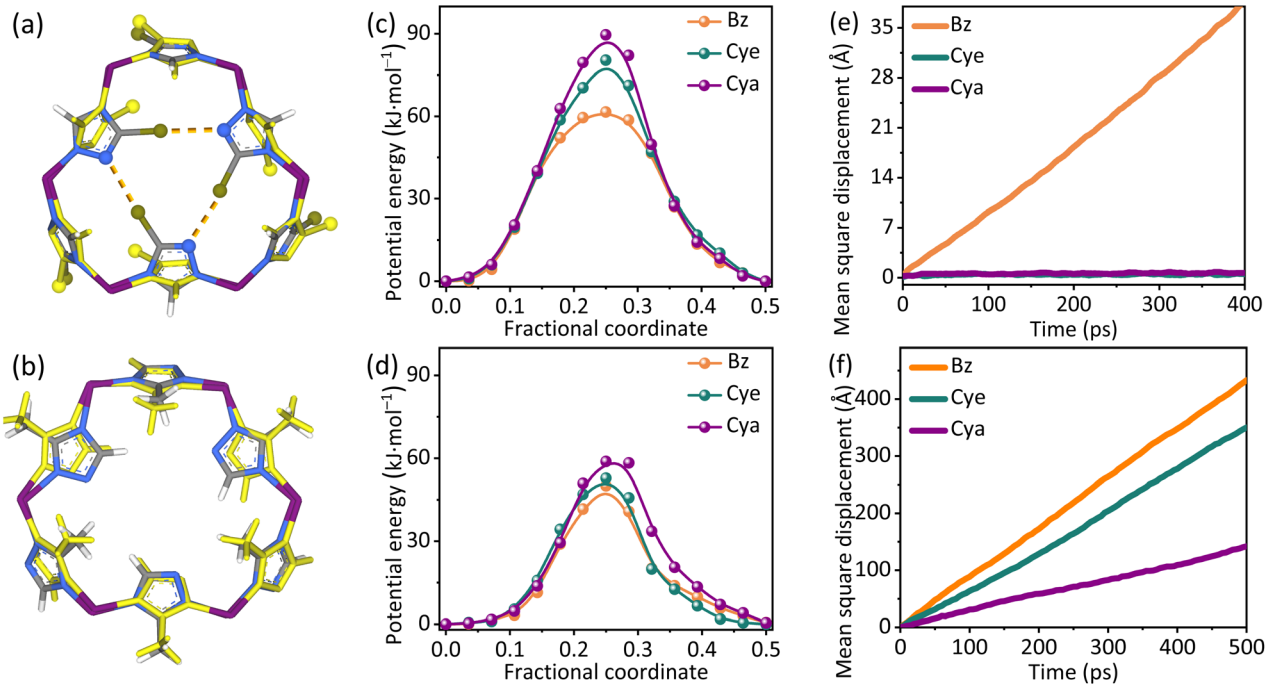

Fig. 4 The simulated gating process and adsorption kinetics. (a and b) The gating moment of the 6 MR aperture in MAF-7Br (a) and MAF-7 (b). (c and d) The gating energy barrier for Bz, Cye and Cya in MAF-7Br (c) and MAF-7 (d). (e and f) MD-derived self-diffusion rates for MAF-7Br (e) and MAF-7 (f).

and 58.8 kJ mol^{-1} for Bz, Cye, and Cya diffusion, respectively (Fig. S44†). For MAF-7Br, because the aperture was much smaller, the ligands rotate ~35.3°, ~37.9°, and ~38.2°, giving energy barriers of 61.6, 80.4, and 89.6 kJ mol^{-1} for Bz, Cye, and Cya, respectively (Fig. S44†).

If the three Br atoms are replaced with H atoms, the gating energy barriers of MAF-7Br become 29.6/47.5/54.5 kJ mol^{-1} for Bz/Cye/Cya, respectively, indicating that the three Br···N interactions contribute *ca.* 33 kJ mol^{-1} (Table S5†). In the absence of Br···N bonds, MAF-7Br exhibits a larger rotation angle and a lower energy increase compared to MAF-7, which can be explained by the steric hindrance at the 4 MR. To open the 6 MR aperture in MAF-7, the triazolate ligands are required to rotate, which causes the 2-methyl groups to come closer in the 4 MR, resulting in significant steric hindrance that increases the energy barrier. In MAF-7Br, the 2-position of the triazolate is H, which largely reduces the steric hindrance for the ligand rotation (Fig S45 and S46†). Overall, the Br···N halogen bond is the key to the significant adsorption kinetic effect and high kinetic selectivity for MAF-7Br.

Conclusions

In summary, we have designed and synthesized a new SOD-MOF. Interestingly, the introduction of halogen bonds not only altered the coordination mode of the linker but also produced a unique gating effect, which allowed the selective adsorption of Bz over Cya/Cye, achieving ultrahigh selectivity for binary/ternary Bz/Cye/Cya separation. Computational simulations demonstrated that the halogen-bonding interaction controlled gating plays a crucial role in molecular-sieving-like Bz/Cye/Cya separation. To our knowledge, hydrogen bonds, coordination bonds, and the hydrophobic effect have been used as gating mechanisms to achieve high-effective adsorptive separation, but this work represents the first example to use halogen bonds for gating. It will open new avenues for exploring more approaches to regulating the framework flexibility and provide a new design strategy for highly efficient separation.

Data availability

The experimental details and datasets supporting this article are available in the ESI.† The crystallographic information can be found in the supplemental materials associated with this work and at the Cambridge Crystallographic Data Center under deposition numbers 2386982 and 2386983.

Author contributions

D. D. Z. and J. P. Z. designed the research. Z. J. L. performed syntheses and measurements. F. D. D. and D. Y. H. performed computational simulations. L. Y. and Z. L. F. performed single-crystal X-ray diffraction analyses. X. F. and M. Y. Z. performed gas chromatography analyses. W. Y. S. and Z. S. W. performed vapour sorption isotherm measurements. K. Z. performed SEM analyses. Z. J. L., D. D. Z., J. P. Z. and X. M. C. wrote the manuscript.

Conflicts of interest

There are no conflicts to declare.

Acknowledgements

This work was supported by the National Natural Science Foundation of China (No. 22090061, 22231012, 22475240, and 22071272).

Notes and references

1 F. Chavarria and D. R. Paul, *Polymer*, 2004, **45**, 8501.
2 T.-B. Wu, P. Zhang, T. Jiang, D.-X. Yang and B.-X. Han, *Sci. China:Chem.*, 2014, **58**, 93.
3 D. S. Sholl and R. P. Lively, *Nature*, 2016, **532**, 435.
4 C. Chen, H.-Y. Guan, H.-B. Li, Y.-Z. Zhou, Y.-G. Huang, W. Wei, M.-C. Hong and M.-Y. Wu, *Angew. Chem., Int. Ed.*, 2022, **61**, e202201646.
5 H. Nagahara, M. Ono, M. Konishi and Y. Fukuoka, *Appl. Surf. Sci.*, 1997, **121**, 448.
6 L. M. C. Silva, S. Mattedi, O. R. Gonzalez and M. Iglesias, *J. Chem. Thermodyn.*, 2006, **38**, 1725.
7 L.-G. Hu, W.-H. Wu, M. Hu, L. Jiang, D.-H. Lin, J. Wu and K. Yang, *Nat. Commun.*, 2024, **15**, 3204.
8 J.-R. Li, R. J. Kuppler and H.-C. Zhou, *Chem. Soc. Rev.*, 2009, **38**, 1477.
9 F. Xie, L.-H. Chen, E. M. C. Morales, S. Ullah, Y.-W. Fu, T. Thonhauser, K. Tan, Z.-B. Bao and J. Li, *Nat. Commun.*, 2024, **15**, 2240.
10 Y.-J. Ding, L. O. Alimi, B. Moosa, C. Maaliki, J. Jacquemin, F.-H. Huang and N. M. Khashab, *Chem. Sci.*, 2021, **12**, 5315.
11 M.-Y. Zhou, X.-W. Zhang, H. Yi, Z.-S. Wang, D.-D. Zhou, R.-B. Lin, J.-P. Zhang and X.-M. Chen, *J. Am. Chem. Soc.*, 2024, **146**, 12969.
12 C.-H. Liu, L.-J. Chen, H. Zhang, Y.-B. Li, H.-Y. Lin, L. Li, J.-J. Wu, C.-L. Liu, Z.-M. Ye, S.-C. Xiang, B.-L. Chen and Z.-J. Zhang, *Chem*, 2023, **9**, 3532.
13 L.-G. Hu, W.-H. Wu, L. Gong, H.-X. Zhu, L. Jiang, M. Hu, D.-H. Lin and K. Yang, *Angew. Chem., Int. Ed.*, 2023, **62**, e202215296.
14 M. Y. Gao, B. Q. Song, D. Sensharma and M. J. Zaworotko, *SmartMat*, 2020, **2**, 38.
15 P. M. Bhatt, V. Guillerm, S. J. Datta, A. Shkurenko and M. Eddaoudi, *Chem*, 2020, **6**, 1613.
16 M. Brian and M. J. Zaworotko, *Chem. Rev.*, 2001, **101**, 1629.
17 M. Dincă and J. R. Long, *Chem. Rev.*, 2020, **120**, 8037.
18 W.-D. Fan, X.-R. Zhang, Z.-X. Kang, X.-P. Liu and D.-F. Sun, *Coord. Chem. Rev.*, 2021, **443**, 213968.
19 A. Kirchon, L. Feng, H. F. Drake, E. A. Joseph and H.-C. Zhou, *Chem. Soc. Rev.*, 2018, **47**, 8611.
20 G.-P. Li, Z.-Z. Li, H.-F. Xie, Y.-L. Fu and Y.-Y. Wang, *Chin. J. Struct. Chem.*, 2021, **40**, 1047.
21 X. Zhang, J. Maddock, T. M. Nenoff, M. A. Denecke, S. Yang and M. Schröder, *Chem. Soc. Rev.*, 2022, **51**, 3243.
22 Y.-P. Han, F. Wang and J. Zhang, *Coord. Chem. Rev.*, 2022, **471**, 214759.

23 A. G. Slater and A. I. Cooper, *Science*, 2015, **348**, aaa8075.
24 L.-H. Xie, M.-M. Xu, X.-M. Liu, M.-J. Zhao and J.-R. Li, *Adv. Sci.*, 2020, **7**, 1901758.
25 J.-P. Zhang and X.-M. Chen, *J. Am. Chem. Soc.*, 2008, **130**, 6010.
26 D.-D. Zhou, P. Chen, C. Wang, S.-S. Wang, Y. Du, H. Yan, Z.-M. Ye, C.-T. He, R.-K. Huang, Z.-W. Mo, N.-Y. Huang and J.-P. Zhang, *Nat. Mater.*, 2019, **18**, 994.
27 Z.-Y. Ji, Y.-R. Fan, M.-Y. Wu and M.-C. Hong, *Chem. Commun.*, 2021, **57**, 3785.
28 J.-M. Wan, H.-L. Zhou, D. Hyeon, K. I.-Y. Chang, Y.-H. Huang, R. Krishna and J.-G. Duan, *Angew. Chem., Int. Ed.*, 2023, **62**, e202316792.
29 A. Schneemann, V. Bon, I. Schwedler, I. Senkovska, S. Kaskel and R. A. Fischer, *Chem. Soc. Rev.*, 2014, **43**, 6062.
30 S. Mukherjee, B. Joarder, B. Manna, A. V. Desai, A. K. Chaudhari and S. K. Ghosh, *Sci. Rep.*, 2014, **4**, 5761.
31 K. Kishida, Y. Okumura, Y. Watanabe, M. Mukoyoshi, S. Bracco, A. Comotti, P. Sozzani, S. Horike and S. Kitagawa, *Angew. Chem., Int. Ed.*, 2016, **55**, 13784.
32 X.-C. Huang, Y.-Y. Lin, J.-P. Zhang and X.-M. Chen, *Angew. Chem., Int. Ed.*, 2006, **45**, 1557.
33 J.-P. Zhang, A.-X. Zhu and X.-M. Chen, *Chem. Commun.*, 2012, **48**, 11395.
34 J. D. Fairen, S. A. Moggach, M. T. Wharmby, P. A. Wright, S. Parsons and T. Düren, *J. Am. Chem. Soc.*, 2011, **133**, 8900.
35 K.-H. Li, D. H. Olson, J. Seidel, T. J. G. Emge, H. Wei, H.-P. Zeng and J. Li, *J. Am. Chem. Soc.*, 2009, **131**, 10368.
36 A. Sławek, K. Roztocki, D. Majda, S. Jaskaniec, T. J. H. Vlugt and W. Makowski, *Microporous Mesoporous Mater.*, 2021, **312**, 110730.
37 L.-H. Yang, Y. Liu, F. Zheng, F.-X. Shen, B. Liu, R. Krishna, Z.-G. Zhang, Q.-W. Yang, Q.-L. Ren and Z.-B. Bao, *ACS Nano*, 2024, **18**, 3614.
38 K. Chen, S. H. Mousavi, R. Singh, R. Q. Snurr, G. Li and P. A. Webley, *Chem. Soc. Rev.*, 2022, **51**, 1139.
39 D. M. Polyukhov, A. S. Poryvaev, S. A. Gromilov and M. V. Fedin, *Nano Lett.*, 2019, **19**, 6506.
40 A. Knebel, B. Geppert, K. Volgmann, D. I. Kolokolov, A. G. Stepanov, J. Twiefel, P. Heitjans, D. Volkmer and J. Caro, *Science*, 2017, **358**, 347.
41 W.-F. Wu, J.-Y. Su, M.-M. Jia, Z.-J. Li, G.-Q. Liu and W.-B. Li, *Sci. Adv.*, 2020, **6**, eaax7270.
42 O. Karagiaridi, M. B. Lalonde, W. Bury, A. A. Sarjeant, O. K. Farha and J. T. Hupp, *J. Am. Chem. Soc.*, 2012, **134**, 18790.
43 Z.-F. Jiang, W.-J. Xue, H.-L. Huang, H.-J. Zhu, Y.-X. Sun and C.-L. Zhong, *Chem. Eng. J.*, 2023, **454**, 140093.
44 C. L. Hobday, T. D. Bennett, J. D. Fairen, A. J. Graham, C. A. Morrison, D. R. Allan, T. Düren and S. A. Moggach, *J. Am. Chem. Soc.*, 2017, **140**, 382.
45 R. Banerjee, A. Phan, B. Wang, C. Knobler, H. Furukawa, M. O'Keeffe and O. M. Yaghi, *Science*, 2008, **319**, 939.
46 X.-C. Huang, J.-P. Zhang and X.-M. Chen, *Chin. Sci. Bull.*, 2003, **48**, 1531.
47 D.-D. Zhou and J.-P. Zhang, *Acc. Chem. Res.*, 2022, **55**, 2966.
48 J.-P. Zhang, A.-X. Zhu, R.-B. Lin, X.-L. Qi and X.-M. Chen, *Adv. Mater.*, 2011, **23**, 1268.
49 L. Zhang, H.-W. Chen, P.-X. Liu, Y. Chen, Y.-T. Liu, R.-B. Lin, X.-M. Chen, J.-P. Li and L.-B. Li, *J. Colloid Interface Sci.*, 2024, **656**, 538.
50 T. D. Bennett and A. K. Cheetham, *Acc. Chem. Res.*, 2014, **47**, 1555.
51 R. Pallach, J. Keupp, K. Terlinden, L. Frentzel-Beyme, M. Kloss, A. Machalica, J. Kotschy, S. K. Vasa, P. A. Chater, C. Sternemann, M. T. Wharmby, R. Linser, R. Schmid and S. Henke, *Nat. Commun.*, 2021, **12**, 4097.
52 R. Pallach, J.-B. Weiß, K. Vollmari and S. Henke, *APL Mater.*, 2023, **11**, 041118.
53 D. Wang and Y. Zhao, *Angew. Chem., Int. Ed.*, 2023, **62**, e202217903.
54 A.-X. Zhu, R.-B. Lin, X.-L. Qi, Y. Liu, Y.-Y. Lin, J.-P. Zhang and X.-M. Chen, *Microporous Mesoporous Mater.*, 2011, **157**, 42.
55 C. Gu, N. Hosono, J.-J. Zheng, Y. Sato, S. Kusaka, S. Sakaki and S. Kitagawa, *Science*, 2019, **363**, 387.
56 Y.-S. Yang, L.-B. Li, R.-B. Lin, Y.-X. Ye, Z.-Z. Yao, L. Yang, F.-H. Xiang, S.-M. Chen, Z.-J. Zhang, S.-C. Xiang and B.-L. Chen, *Nat. Chem.*, 2021, **13**, 933.
57 Q. Gao, J. Xu, D.-P. Cao, Z. Chang and X.-H. Bu, *Angew. Chem., Int. Ed.*, 2016, **55**, 15027.